Science of the Total Environment 923 (2024) 171527

Contents lists available at ScienceDirect

Science of the Total Environment

journal homepage: www.elsevier.com/locate/scitotenv

Interannual variations in ozone pollution with a dipole structure over Eastern China associated with springtime thermal forcing over the Tibetan Plateau

Qingjian Yang [a], Tianliang Zhao [a,*], Yongqing Bai [b], Jing Wei [c], Xiaoyun Sun [a], Zhijie Tian [d], Jun Hu [e], Xiaodan Ma [a], Yuehan Luo [a], Weikang Fu [a], Kai Yang [a]

[a] *Climate and Weather Disasters Collaborative Innovation Center, Key Laboratory for Aerosol-Cloud-Precipitation of China Meteorological Administration, PREMIC, Nanjing University of Information Science &Technology, Nanjing 210044, China*
[b] *Institute of Heavy Rain, China Meteorological Administration, Wuhan 430205, China*
[c] *Department of Atmospheric and Oceanic Science and ESSIC, University of Maryland, College Park, MD, USA*
[d] *China Institute for Radiation Protection, Taiyuan 030006, China*
[e] *Fujian Academy of Environmental Sciences, Fuzhou 350011, China*

HIGHLIGHTS

- The TP thermal forcing modulates the interannual variations in O_3 pollution over EC.
- Strong TP forcing worsens and reduces O_3 pollution in the northern and southern EC.
- The mechanism of TP thermal forcing effect on O_3 pollution change in EC is revealed.

GRAPHICAL ABSTRACT

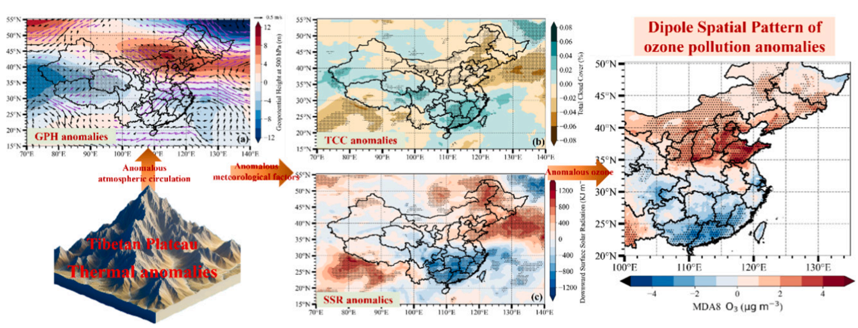

ARTICLE INFO

Editor: Anastasia Paschalidou

Keywords:
Thermal anomalies
Ozone change
Spatial pattern
Climate variability

ABSTRACT

The Tibetan Plateau (TP) is essential in modulating climate change in downstream Eastern China (EC). As a meteorology-sensitive pollutant, changes in ozone (O_3) in connection with the TP have received limited attention. In this study, using climate analysis of the China High Air Pollutants O_3 product and ERA5 reanalysis data of meteorology for 1980–2020, the effect of springtime TP thermal forcing on the warm season (April–September) O_3 pollution over EC was investigated. The strong TP thermal effect significantly modulates the interannual variations in O_3 pollution with a dipole pattern over EC, inducing more O_3 pollution in northern EC regions and alleviating O_3 pollution in the southern regions. In northern (southern) EC, strong TP thermal forcing triggers a significant anomalous high (low) pressure center accompanied by anticyclonic (cyclonic) anomalies, resulting in decreased (increased) total cloud cover, increased (reduced) surface downward solar radiation and air temperature, which are conducive to the anomalous increase (decrease) in surface O_3 concentrations. Moreover, the key sources of springtime thermal forcing over the TP influence the major O_3 pollution regions over southern and

* Corresponding author.
E-mail address: tlzhao@nuist.edu.cn (T. Zhao).

https://doi.org/10.1016/j.scitotenv.2024.171527
Received 28 December 2023; Received in revised form 2 March 2024; Accepted 4 March 2024
Available online 5 March 2024

northern EC with an inverse pattern, depending on their locations and orientations to the large topography of the TP. This research reveals an important driving factor for the dipole interannual variation in O_3 pollution over EC, providing a new prospect for the effect of the TP on atmospheric environmental change.

1. Introduction

Tropospheric ozone (O_3) has attracted considerable attention and research interest worldwide (Wang et al., 2022) as a strong oxidant detrimental to human health (Nuvolone et al., 2018; Wang et al., 2021a), crop growth (Feng et al., 2015), and ecosystems (Yue et al., 2017). Although it has been widely confirmed that tropospheric O_3 is produced via the photochemical oxidation of volatile organic compounds and nitrogen oxides (Sillman, 2003), understanding the spatiotemporal variations in O_3 remains challenging because of its abundant precursor sources, complex reaction mechanisms, and numerous meteorological factors (Li et al., 2019a).

Although anthropogenic emissions of O_3 precursors are the primary drivers of O_3 increases in China (Ma et al., 2023), meteorological conditions are also crucial in O_3 changes, with a contribution rate of 43 % in Eastern China (EC) (Han et al., 2020). Meteorological conditions affect the surface O_3 via various pathways (Jacob and Winner, 2009; Lin et al., 2008; Shen et al., 2016). For example, strong solar radiation can accelerate the atmospheric photochemical production of O_3 (Lu et al., 2019a; Ma et al., 2019), high air temperatures can enhance the chemical formation rates of O_3 (Lee et al., 2014), and suppressed planetary boundary layer height can restrain upward movement thereby reducing surface O_3 concentrations (Haman et al., 2014). Meteorological conditions impose a composite effect on O_3 pollution and are modulated by various external climatic forces, including that of the Tibetan Plateau (TP).

With an average elevation of >4000 m and occupying one-fourth of the total land area of China, the large topography of the TP significantly affects the weather and climate in East Asia (Wu et al., 2007). In spring and summer, the "elevated air pump" effect of the TP (Wu et al., 2018) generates a large-scale heat source over the TP, regulating the East Asian summer monsoon and the meteorological conditions in EC (Ma et al., 2017; Wu et al., 2012a, 2012b). In terms of the climate scale, interannual variations in TP thermal forcing have led to regional climate change patterns in China. In the years with the positive anomalies of TP thermal forcing, the summer monsoon precipitation is spatially characterized by the anomalous pattern of "north wet–south dry" over EC, with the reverse precipitation change pattern in the years of the negative anomalies of the TP thermal forcing (Xu et al., 2013). The interannual increase in diabatic heating in the TP can strengthen the upper-tropospheric South Asia high and downstream subtropical high, thus modulating meteorological conditions in downstream regions (Bao et al., 2008). Consequently, through the impact on meteorological conditions, interannual variations in air pollution over EC are inevitably affected by TP thermal forcing. Thermal anomalies over the TP lead to frequent haze events in EC by intensifying downward air flows and increasing local atmospheric stability (Xu et al., 2016). Anomalous high springtime TP thermal forcing is conducive to reducing O_3 concentrations in central China through anomalous transport under favorable weather conditions (Wang et al., 2021b).

Many studies have confirmed that TP thermal forcing has a lag effect on circulation and weather conditions in China (Duan et al., 2011; Duan and Wu, 2005; Ge et al., 2019; Wang et al., 2014; Zhao et al., 2007). For instance, the springtime TP thermal forcing can influence summer precipitation over EC through atmospheric circulation patterns (Liu et al., 2007), water vapor transportation (Xu et al., 2013), the western North Pacific subtropical high (Zhang et al., 2018), and land-sea thermal contrast (Han et al., 2024), altering the meteorological elements for O_3 pollution in the downstream EC. However, the relationship between the TP thermal effect and regional O_3 pollution in EC in the interannual variations remains unclear, particularly with the impact of springtime TP thermal forcing on the subsequent warm season O_3 pollution in EC.

In this study, the impact of interannual springtime TP thermal forcing on O_3 pollution in EC was investigated using a long-term O_3 dataset and meteorological reanalysis data. The aim of this study was to extend the environmental influence of the TP forcing on O_3 pollution over downstream regions for a comprehensive understanding of environmental changes in China.

2. Data and methodology

2.1. Data

The monthly maximum daily average 8 h (MDA8) O_3 product with full coverage across China from 1980 to 2020 at a horizontal resolution of 0.1° × 0.1° was obtained from the China High Air Pollutants (CHAP) dataset (https://weijing-rs.github.io/product.html). This dataset was generated from core input predictors (i.e., downwelling surface solar radiation and surface air temperature), together with other big data including observations, satellites, and models, by employing a space-time extremely randomized trees machine learning model. The out-of-sample10-fold cross-validation method and main statistical metrics between the CHAP data and the available field observations over China were used to evaluate the CHAP data accuracy by one of our authors, Wei Jing (Wei et al., 2022). The CHAP dataset exhibits good performance in the root-mean-square error (RMSE) of 17.10 μg m^{-3}, mean absolute error (MAE) of 11.29 μg m^{-3}, and mean relative error (MRE) values of 18.38 % in the daily validation over the entire domain (Wei et al., 2022), which would not influence the reasonable analysis on climatic change (He et al., 2022). Therefore, the CHAP data with reasonable overall accuracy was utilized in this climatic study on interannual variations in O_3 pollution for 1980–2020 over Eastern China with the effects of the Tibetan Plateau thermal forcing.

The monthly meteorological data with a spatial resolution of 0.25° × 0.25° were derived from the ERA5 (Hersbach et al., 2020) reanalysis dataset (https://www.ecmwf.int/en/forecasts/datasets/reanalysis-datasets/era5/), including 850 hPa wind fields, temperature at 2 m (T2), geopotential height at 500 hPa (Z500), downward surface solar radiation (SSR), and total cloud cover (TCC).

2.2. The heat source over the TP

The atmospheric heat source (Q1) is a physical quantity that reflects the heat balance of an air column. For a given area, the Q1 is defined as the heat gained (lost) by the air column over a period of time, which is a combination of sensible heat, latent heat of condensation, and atmospheric radiation. Following the inverse algorithm of Yanai et al. (1973, 1992), the Q1 was calculated based on the ERA5 reanalysis data:

$$Q_1 = c_p\left[\frac{\partial T}{\partial t} + V\cdot\nabla T + \left(\frac{p}{p_0}\right)^k \omega\frac{\partial \theta}{\partial p}\right] \quad (1)$$

where T and θ are the temperature and potential temperature, respectively; ω is the vertical velocity; k = R/Cp, where R and Cp are the dry air gas constant and specific heat at constant pressure, respectively; V is the horizontal wind vector; and P_0 is 1000 hPa. The three terms to the right of the equation are the local variation, horizontal advection, and vertical transport terms.

The vertical integral value of Q1 can be expressed as:

$$\langle Q_1 \rangle = \frac{1}{g}\int_{p_t}^{p_s} Q_1 dp \quad (2)$$

where P_s and P_t denote the surface pressure and atmospheric top pressure (200 hPa), respectively, and g is gravitational acceleration. The vertical integral of Q1 represents the atmospheric thermal conditions over a certain region, with positive values of Q1 denoting heating and negative values denoting cooling. The regionally averaged Q1 over the TP area of 78–103°E and 28–38°N, covering most of the region with an altitude >3000 m (Xu et al., 2016), represents the thermal forcing of the TP (TP-Q1).

2.3. Wavelet analysis

Morlet wavelet analysis is a common tool for analyzing long-term changes in variables, and is spreading to studies of interannual changes in climate factors (Anctil and Coulibaly, 2004; Coulibaly et al., 2000). It is used for frequency- and time-domain analyses of nonstationary time series that cannot be analyzed using standard methods (Sifuzzaman et al., 2009). The Morlet wavelet primarily uses the localization characteristics to identify various change cycles hidden in the time series and fully reflects the changing trend of a variable at different time scales (Tang et al., 2023). The calculation method for the Morlet wavelet is detailed in Torrence and Compo (1998). In this study, wavelet analysis was used to identify the interannual change circles of springtime TP-Q1.

2.4. Butterworth filter

After the wavelet analysis, the Butterworth filter was applied to extract the 1–4-year signal of springtime TP-Q1, following the method of Gouirand et al. (2012). The Butterworth filter is a type of signal-processing filter designed to have a smooth and monotonic decrease in amplitude as the frequency increases without oscillations. It can be implemented as a low-, high-, and band-pass filter, depending on the desired frequency range. Since it was first described in 1930 by Stephen Butterworth (Butterworth, 1930), it has been widely used in meteorology and climate analyses (Gouirand et al., 2012; Yang et al., 2021; You and Liang, 2017), because it can filter out unwanted frequencies while preserving the original signal shape.

2.5. Empirical orthogonal function (EOF)

EOF analysis has been widely used in meteorological studies to analyze the spatial and temporal variability of physical fields (Hannachi et al., 2007). It decomposes a spatial-temporal dataset into space eigenvectors (EOFs) and corresponding time coefficients (PCs), which can identify the spatial modes of the variables and the amplitude of each EOF mode over time, respectively. In this study, the EOF method was used to identify the main patterns of interannual MDA8 O_3 variations to determine the relationship between changes in springtime TP thermal forcing and EOF modes.

3. Results and discussion

3.1. Spatial distribution and seasonality of O_3 pollution

The EC region (100–135°E, 20–50°N), with >70 % of the Chinese population, experiences the most frequent occurrence of O_3 pollution in China (Wang et al., 2022). From north to south, there are six densely populated subregions in EC (1–6 in Fig. 1a): northeast China (NEC; 120–126°E, 40–45°N), the North China Plain (NCP; 114–120°E, 34–42°N), the Sichuan Basin (SB; 103–108°E, 28–32.5°N), the Central China (CC; 112–116°E, 29–32.5°N), the Yangtze River Delta (YRD; 118–122.5°E, 29–33°N), and the Pearl River Delta (PRD; 112–116°E, 22–25°N).

Examination of monthly MDA8 O_3 concentrations averaged from 1980 to 2020 over EC indicated that O_3 pollution (characterized by MDA8 O_3 concentrations) in EC oscillates seasonally between the peak in summer and the valley in winter (Fig. 1b). High MDA8 O_3 concentrations mainly occur in the warm season from April to September, including three months with MDA8 O_3 concentrations >100 μg m^{-3} (May, June, and July). Meanwhile, other months (October to March) with relatively slight O_3 pollution have MDA8 O_3 concentrations <80 μg m^{-3}, with December recording the lowest value. Therefore, our research focused on O_3 pollution during the warm season.

The climatic spatial pattern of O_3 pollution for the warm seasons of 1980–2020 (Fig. 1a) reveals that the MDA8 O_3 concentrations in most EC areas exceed 100 μg m^{-3}. The six densely populated urban agglomerations were regions with relatively serious O_3 pollution. Among these, the NCP suffers the most serious O_3 pollution with a regional averaged MDA8 O_3 concentration of 121.50 μg m^{-3} (Table 1), followed by NEC, the YRD, and CC (~104 μg m^{-3}), and the SB and PRD (~90 μg m^{-3}). Severe O_3 pollution in the six subregions has been a research hotspot for several years; however, few studies have revealed its relationship with the TP thermal effect, which is the focus of the present study.

3.2. Interannual variations in O_3 pollution

The trend and change rate (CR) were calculated to identify the characteristics of interannual variations in O_3 pollution. The CR was obtained by dividing the trends with averaged MDA8 O_3 concentrations over 41 years, which is more responsive to the relative change characteristic of pollutants in a given region (Sun et al., 2023).

The spatial distribution of the CR indicates that O_3 pollution in EC has become increasingly serious over the past 41 years, with positive CR

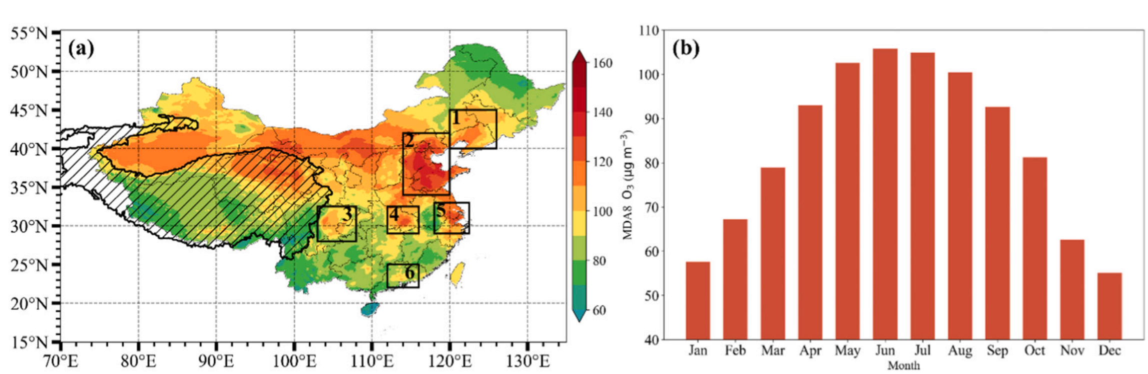

Fig. 1. (a) Distribution of MDA8 O_3 concentrations over the mainland of China averaged for the warm seasons of 1980–2020 (color shading). The TP is marked with oblique lines. Black boxes with numbers 1, 2, 3, 4, 5, and 6 denote the NEC, NCP, SB, CC, YRD, and PRD regions, respectively. (b) Monthly variation in MDA8 O_3 concentrations (μg m^{-3}) over EC averaged from 1980 to 2020.

Table 1
Averages, linear trends, and change rates (trends/averages*100 %) in interannual variations in regional averaged MDA8 O_3 concentrations over the NEC, NCP, SB, CC, YRD, and NEC regions for the warm seasons of 1980–2020.

Regions	Averages (μg m^{-3})	Trends (μg m^{-3} y^{-1})	Change rates (% y^{-1})
NEC	104.54	0.18	0.17
NCP	121.50	0.23	0.19
YRD	104.25	0.17	0.16
CC	103.66	0.26	0.25
SB	93.81	0.23	0.25
PRD	87.30	0.26	0.30

values in most EC areas (Fig. 2). The high CR values were primarily situated in central and southern EC, a pattern that contrasts with the spatial distribution of averaged MDA8 O_3 concentrations (Fig. 1a), indicating that attention should be given to the areas characterized by low concentrations of pollutants that are exhibiting high growth rates.

The regional averaged MDA8 O_3 concentrations exhibited a significant increasing trend at the 95 % confidence level (Fig. S1) for the six subregions, with the highest trend in the PRD and CC of 0.26 μg m^{-3} yr^{-1}, followed by SB and NCP, and the YRD and NEC (Table 1). Although the trend in the NCP ranked second among the six regions, in view of having the most serious O_3 pollution, its CR was relatively low. The trend and CR in the PRD were both highest among the six regions, despite the regional averaged MDA8 O_3 concentration in the PRD being the lowest among the EC regions, its high growth rate also warrants attention. Notably, the regional averaged MDA8 O_3 concentrations in all six regions increased rapidly after 2015 (Fig. S1). The combined effect of decreasing NOx emissions and $PM_{2.5}$ concentrations (Li et al., 2019b; Wang et al., 2020) and favorable meteorological variations (Li et al., 2020; Wei et al., 2022) contributed to the significant increase after the implementation of Clean Air Action initiated by the Chinese government in 2014.

In conclusion, there were significant differences in the spatiotemporal variations in O_3 pollution in the EC regions. As EC is the "susceptible region" of atmospheric environmental change to the large topography of the TP (Xu et al., 2016), the severe O_3 pollution in northern EC and the high growth rate in the south may both be affected by the TP thermal effect, which is explored in the next sections.

3.3. Identifying the TP springtime thermal effect on EC O_3 pollution

3.3.1. Patterns of TP thermal effect on O_3 pollution changes over EC

According to the Morlet wavelet analysis, the interannual change circles of springtime TP-Q1 were identified. Fig. 3a shows the primary change period (left axis) of TP-Q1 from 1980 to 2020 (bottom axis).

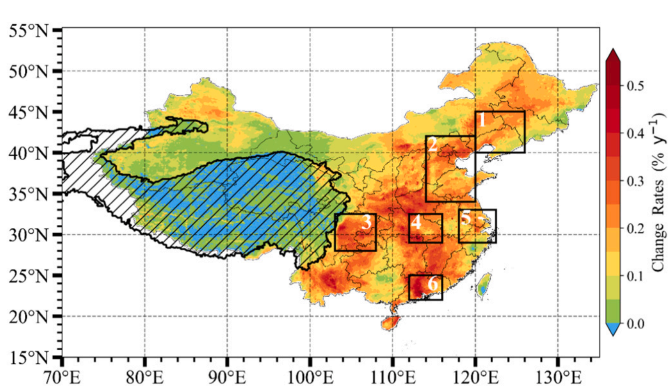

Fig. 2. Distribution of the interannual change rates (trends/averages*100 %, % yr^{-1}) in MDA8 O_3 concentrations over the mainland of China for the warm seasons of 1980–2020. The TP is marked with oblique lines. Black boxes with numbers 1, 2, 3, 4, 5, and 6 denote the NEC, NCP, SB, CC, YRD, and PRD regions, respectively.

According to the powers with a 95 % significance level (bold black contours), the 2–3-year change circle mainly appeared between 1985 and 1995, the 1–3-year change circle mainly appeared after 2000, and the 4-year period was identified between 1980 and 2020 except the years around 2000. Consequently, the 1–4-year large powers dominated from 1980 to 2020, passing the 95 % significance level. The global wavelet spectrum (blue solid line in Fig. 3b) reflects the change period of TP-Q1 from the perspective of all 41 years, which also has an obvious power peak in a 4-year period at a 95 % significance level. Both spectra revealed a substantial change signal of Q1 below 4 years, indicating that the high-frequency (1–4 years) variation in springtime TP-Q1 dominated the change characteristics.

To clarify how the dominant interannual anomalies of TP thermal forcing affect O_3 pollution over EC, the 1–4-year signal of springtime TP-Q1 (Q1_IA) was obtained using a Butterworth filter (Gouirand et al., 2012). As shown in Fig. 4a, the normalized Q1_IA variation pattern was generally consistent with the original TP-Q1 change over the 41 springs, showing more pronounced interannual variations as the wavelet power spectra suggested a dominant contribution of the high-frequency (1–4 years) variations to the TP-Q1 changes during 1980–2020. Considering that all variables should have a consistent interannual signal (Sun and Guan, 2021; Zhu et al., 2021), the same filtering method was applied to MDA8 O_3 (Fig. 4b) and related meteorological factors. Kou et al. (2023) indicated that global warming is conducive to more frequent O_3 pollution on a climate scale. Wang et al. (2021b) revealed that the surface O_3 long-term trend over entire China during 1950–2019 was mainly contributed by anthropogenic emissions. As a result, the 1–4-year filter can basically remove the impact of global warming and anthropogenic emissions, which dominate the filtered-out variation components in O_3 pollution in the long term beyond 1–4 years. Thus, after data preprocessing, high-frequency variations in Q1 and MDA8 O_3 are discussed in detail in the following sections. Hereafter, the variations in Q1 over the TP and MDA8 O_3 over the EC are referred to as Q1_IA and MDA8 O_3_IA, respectively.

To determine the relationship between the TP thermal effect and O_3 pollution, a composite analysis was utilized to explore the spatial patterns of O_3 pollution between the strong and weak Q1 years. Based on the normalized Q1_IA (Fig. 4a), years with a Q1_IA greater and less than one standard deviation were selected as strong and weak Q1 years, respectively. Thus, seven strong years (1985, 1989, 1994, 1997, 2010, 2012, and 2017) and seven weak years (1986, 1988, 1990, 1995, 1998, 2011, and 2018) were identified. The composite anomalies of MDA8 O_3_IA during strong Q1 years (Fig. 5a) showed an obvious dipole spatial pattern with positive anomalies in northern EC but negative anomalies in southern EC, whereas the composite anomalies of MDA8 O_3_IA during weak Q1 years (Fig. 5b) showed an opposite distribution. The difference between the strong and weak Q1 years (strong - weak) had a more prominent spatial dipole pattern (Fig. 5c), with higher and lower anomalous values, respectively, and larger areas passing the significance test. During strong Q1 years, the focal point of positive anomalies (>3 μg m^{-3}) was primarily situated within the NCP, an area noted for the most severe O_3 pollution among EC regions (Fig. 2b), indicating the necessity for implementing stricter measures in the NCP to alleviate the O_3 pollution under strong TP thermal forcing.

Further analysis on the distributions of correlation coefficients (R) of MDA8 O_3_IA to Q1_IA (Fig. 5d) also confirmed that springtime TP thermal forcing led to a dipole spatial distribution; the strong thermal forcing brought more O_3 pollution to the northern EC regions but alleviated the O_3 pollution in southern regions. Regarding the SB, CC, and YRD regions situated in the Yangtze River basin around 30°N, identified as the transitional zone displaying positive and negative R values, it appears that these regions are less influenced by the thermal anomalies of the TP or different TP areas have opposite effects on these regions, which will be explored in a later section.

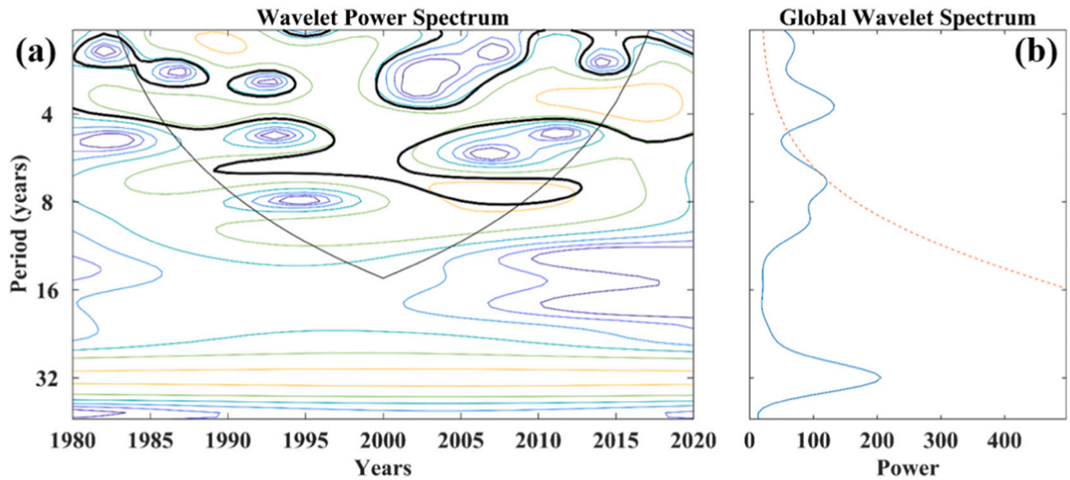

Fig. 3. (a) Wavelet power spectrum of springtime TP-Q1 over 41 years using the Morlet wavelet analysis. The contours indicate wavelet powers in which the bold black contour lines enclose peaks of >95 % confidence. (b) The global wavelet spectrum for the interannual variation in springtime TP-Q1. The red dashed line indicates the red noise with a 95 % confidence level.

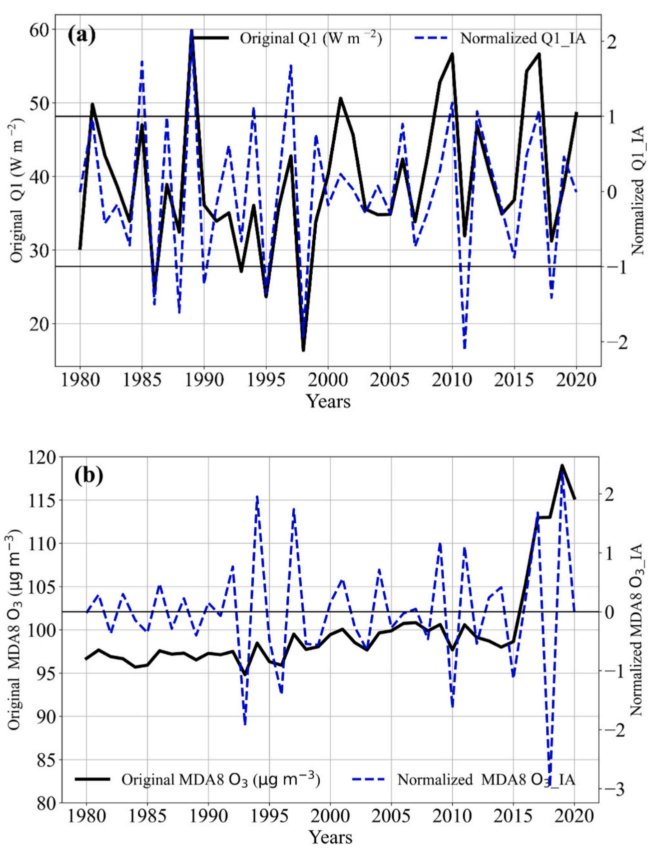

Fig. 4. Interannual variations in (a) springtime TP-Q1 with the filtered and normalized interannual component (Q1_IA), (b) MDA8 O_3 concentrations averaged over EC for the warm seasons of 1980–2020 with its filtered and normalized interannual component (MDA8 O_3_IA).

3.3.2. The EOF pattern of O_3 pollution variations associated with TP-Q1

EOF analysis was performed on MDA8 O_3_IA over the EC regions to further identify the dominant patterns of interannual spatiotemporal variations in O_3 pollution and their relationship with the springtime TP thermal effect. The variance contributions of the first two leading modes were 29.25 % and 19.73 %, passing the North significance test, and the two modes were significantly separated. The spatial patterns of the first EOF were identified as a uniform change in most EC regions (Fig. S2), whereas those of EOF2 showed a dipole feature with negative values in the southern regions but positive values in the northern regions, both of which exhibited significant interannual fluctuations in PC values (Fig. 6).

Various complex climatic factors may contribute to the EOF pattern of O_3 pollution (Gao et al., 2023; Ma and Yin, 2021), while few studies have demonstrated their connection to TP thermal forcing. Correlation analysis between springtime Q1_IA and PC1 (PC2) showed that the R-value between Q1_IA and PC1 was 0.21, which failed the significance test. However, the R-value between Q1_IA and PC2 reached 0.52, passing the 99 % significance level. The close relationship between Q1_IA (black dashed line in PC2) and PC2 further confirms that TP thermal forcing may modulate the dipole distribution of O_3 pollution in the EC regions; strong and weak springtime TP thermal forcing leads to more and less O_3 pollution in the northern and southern EC regions, respectively.

3.3.3. Key TP heat sources to regional O_3 pollution

As an extensive region occupying 25 % of the total land area of China, the TP has complex weather and environmental conditions, and heat sources over the TP also have spatial heterogeneity. Because springtime TP thermal forcing substantially impacts O_3 pollution in EC, identifying the key heat sources over the TP for different EC subregions is helpful for intensive studies on the connection between Q1 over a specific TP area and severe O_3 pollution in a certain region.

The R values of the warm season averaged MDA8 O_3_IA over the SB, CC, YRD, NEC, NCP, and PRD regions with the prior springtime Q1_IA in the same year over the TP were calculated to present respectively their spatial patterns of thermal forcing anomalies over the TP (Fig. 7b–g). Located zonally downstream of the TP, the key sources of thermal forcing over the TP for the SB (Fig. 7b), CC (Fig. 7c), and YRD (Fig. 7d) present the general patterns of "positive-negative-positive" staggered distribution from west to east. The dominant negative correlations were centered over the central and eastern TP (Fig. 7b–d), demonstrating the key sources of thermal forcing with springtime negative anomalies leading to warm season more O_3 pollution over the zonally downstream of the TP. Differently, the interannual changes of O_3 pollution in the NEC (Fig. 7e), NCP (Fig. 7f), and PRD (Fig. 7g), located in areas affected by the detouring air flow of westerlies generated by the large topography of the TP, present distinct source distributions of thermal forcing anomalies. For the NEC and NCP, there were positive correlations covering from west to east in the TP, and the key sources for the NCP were more prominent in the eastern TP, indicating springtime positive anomalies

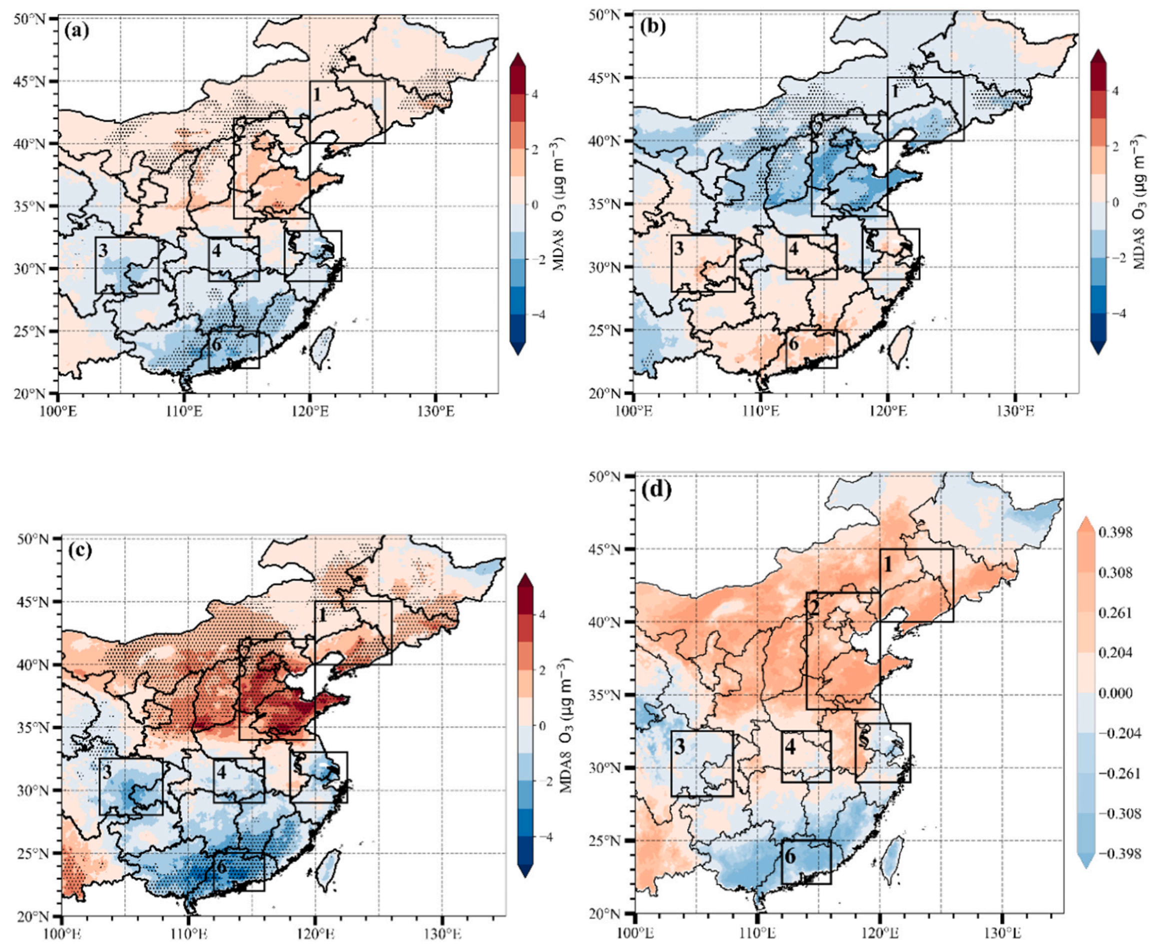

Fig. 5. Composite anomalies of MDA8 O_3_IA (μg m^{-3}) during (a) strong Q1 years, (b) weak Q1 years, and (c) their differences. Black dots indicate that the anomalies are statistically significant at the 95 % confidence level based on the Student's *t*-test. (d) Distributions of R values of MDA8 O_3_IA to the regionally averaged Q1_IA over the TP; the R values of 0.204 (−0.204), 0.261 (−0.261), 0.308 (−0.308), and 0.398 (−0.398) pass the 80, 90, 95, and 99 % significance levels, respectively. Black boxes with numbers 1, 2, 3, 4, 5, and 6 denote the NEC, NCP, SB, CC, YRD, and PRD regions, respectively.

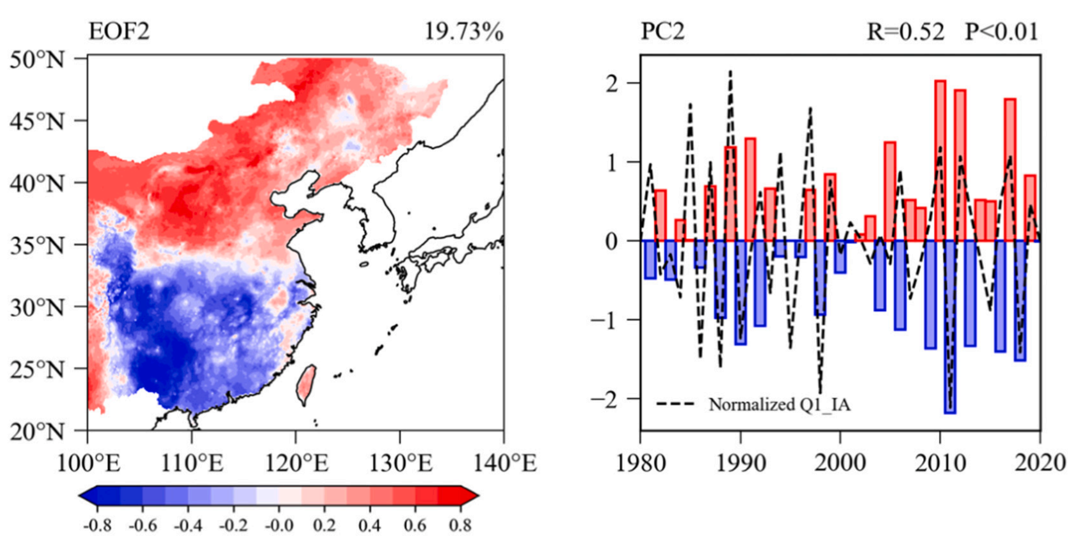

Fig. 6. Spatial pattern (left panel) and principal component (right panel) of the second EOF mode of MDA8 O_3_IA over EC for the warm seasons of 1980–2020. The black dashed line in PC2 denotes Q1_IA.

leading to warm season more O_3 pollution over the detouring air flow regions in the TP northern side. However, For the PRD in the TP southern side detouring air flow regions, significant negative correlations were identified in the southern and eastern TP, exhibiting the inverse pattern of thermal forcing anomalies over TP with northern China. Basically, the key sources of thermal forcing over the TP

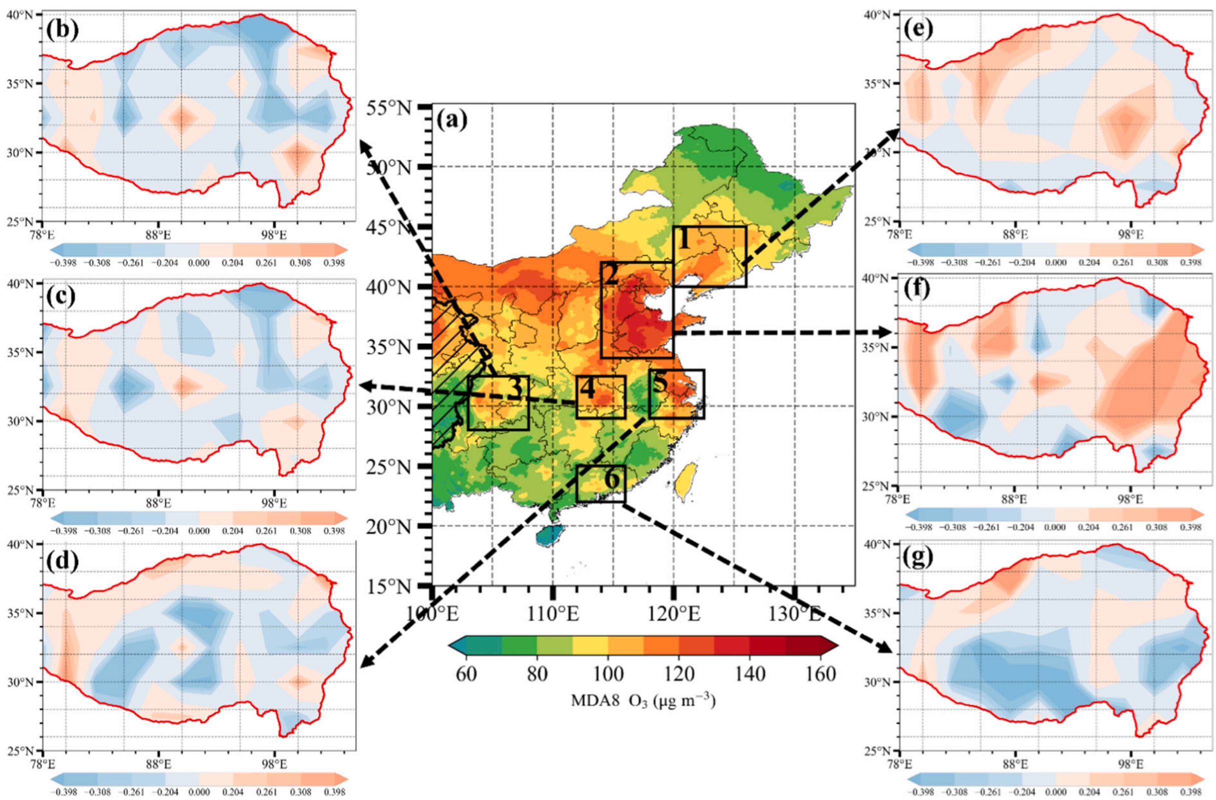

Fig. 7. (a) Same as Fig. 1a, (b–g) distributions of R values of interannual variations in the regionally averaged MDA8 O_3_IA over the SB, CC, YRD, NEC, NCP, and PRD to the Q1_IA over the TP. The R values of 0.204 (−0.204), 0.261 (−0.261), 0.308 (−0.308), and 0.398 (−0.398) pass the 80, 90, 95, and 99 % significance levels, respectively.

influenced the major O_3 pollution regions in southern and northern EC with the inverse pattern, depending on their locations and originations to the large topography of the TP, which could result in the interannual variations in O_3 pollution with a dipole structure over EC.

The interannual changes in springtime TP thermal forcing are associated with various climate factors (Duan and Zhang, 2022). For example, the North Atlantic tripole pattern sea surface temperature anomaly can reduce atmospheric heat source over the southern TP through the modulation on subtropical westerly jet (Cui et al., 2015). The negative phase of the Indian Ocean Basin Mode could enhance the atmospheric heat source over the eastern TP by altering the Hadley circulation (Zhao et al., 2018). The surface factors over the TP also contribute to the regional changes in springtime TP thermal forcing, such as the snow cover areas and depth with spatial heterogeneity over the TP (Ping and Longxun, 2001). Consequently, considering the spatially heterogeneous nature of interannual changes in the springtime thermal forcing over the TP, the key heat sources identified in this study could be used in the more effective and fine prediction of O_3 pollution in major air pollution regions.

3.4. Meteorological mechanism of TP thermal effect

To unravel the underlying mechanisms driving the dipole distribution of O_3 pollution in EC due to TP thermal forcing, a composite analysis was conducted between strong and weak Q1 years in the Z500 and 850 hPa wind fields to examine the anomalous atmospheric circulation associated with the thermal effect. The composite difference (Fig. 8a) revealed that strong TP thermal forcing led to a significant anomalous high-pressure center at 500 hPa and an anomalous anticyclone at 850 hPa in northern EC. Conversely, in southern EC, strong TP thermal forcing triggered an anomalous low-pressure center and cyclone. The dipole structure of anomalous atmospheric circulation exerts opposing influences on the synoptic patterns in northern and southern EC, thereby modulating local meteorological factors differently.

The presence of an anomalous high-pressure system promotes downdrafts and stagnant atmospheric conditions that are unfavorable for cloud formation. Further examination of the composite difference in the TCC confirmed a dipole spatial pattern corresponding to anomalous circulation, with negative anomalies in northern EC but positive anomalies in southern EC (Fig. 8b). The anomalously strong TP thermal forcing was conducive to the reduction of TCC in northern EC but enhancement in southern EC.

Thick clouds weaken the SSR reaching the ground through absorption and reflection, causing a reduction in SSR and T2. SSR and T2 are the most direct meteorological factors affecting O_3 concentrations by accelerating atmospheric photochemical and thermochemical production and enhancing the natural emissions of O_3 precursors from vegetation and soil (Gu et al., 2020; Lu et al., 2019; Ma et al., 2019). Compared to weak Q1 years, strong Q1 years exhibited a dipole structure in SSR and T2 anomalies, with positive anomalies in northern EC and negative anomalies in southern EC (Fig. 8c, d). Anomalous high (low) SSR and T2 in the northern (southern) EC accelerated (suppressed) local photochemical production of O_3, leading to positive (negative) MDA8 O_3 anomalies.

In summary, strong TP thermal forcing triggers a significant anomalous high (low) pressure center accompanied by an anticyclone (cyclone), resulting in reduced (increased) TCC, increased (reduced) SSR and T2, and a resultant anomalous increase (decrease) in MDA8 O_3 concentrations in northern (southern) EC. In addition, Relative humidity (RH) and precipitation (PRECI) are also essential factors affecting local O_3 pollution. RH can influence the OH radicals and the heterogeneous reactions of O_3 (He et al., 2017; Li et al., 2021), PRECI can reduce solar radiation, and scavenge O_3 and its precursors in the atmosphere

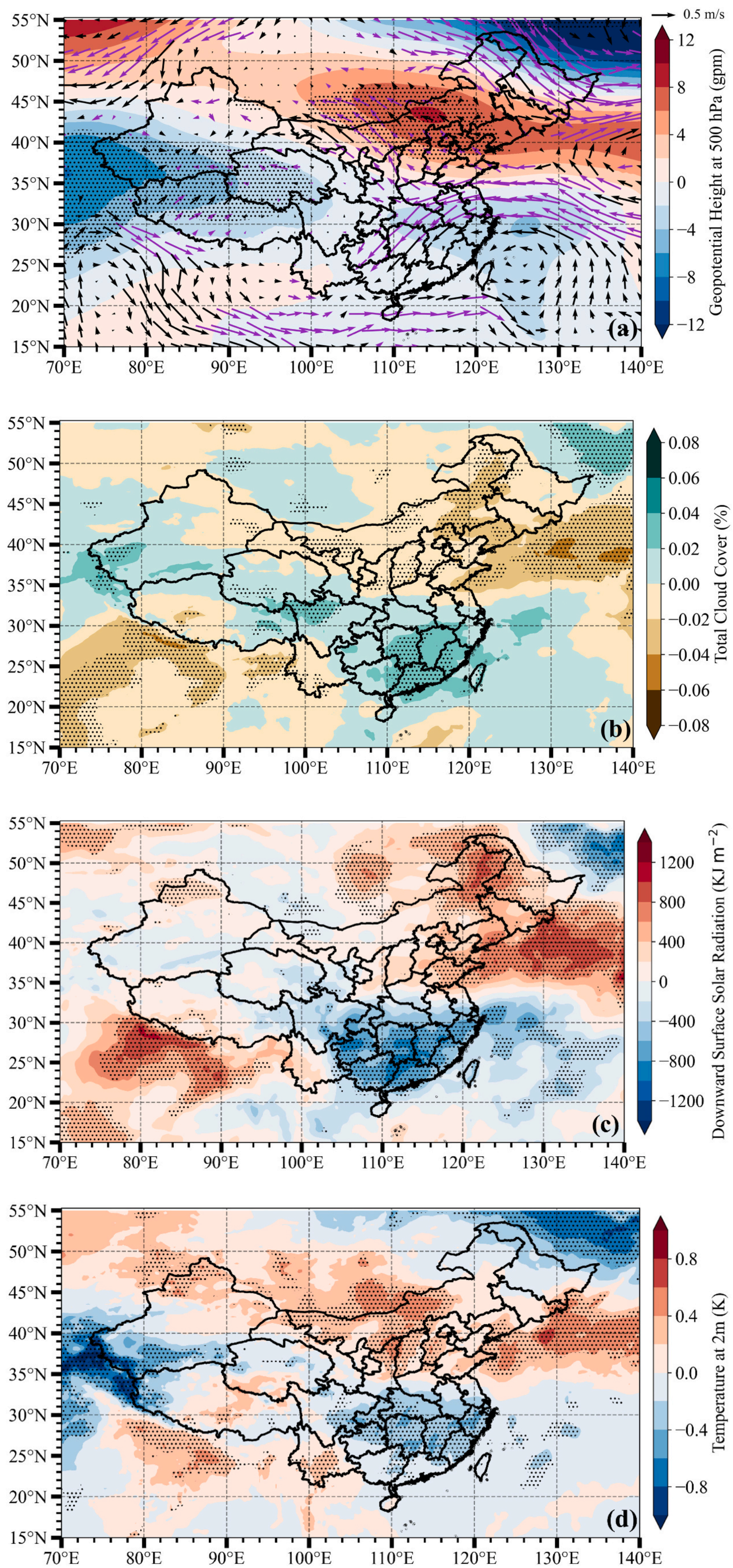

Fig. 8. Composite differences in (a) geopotential height at 500 hPa (shading, gpm) and wind field at 850 hPa (vectors, m s^{-1}), (b) total cloud cover (%), (C) downward surface solar radiation (KJ m^{-2}), and (d) air temperature at 2 m (K). Black dots and purple vectors indicate the composite anomalies passing the 95 % confidence level based on the Student's *t*-test.

(Arshinova et al., 2019; Lu et al., 2019). Therefore, we further included relevant analysis in Fig. S3. The composite difference in the RH2 and PRECI also confirmed a dipole spatial pattern corresponding to anomalous circulation, with negative anomalies in northern EC but positive anomalies in southern EC.

4. Conclusions

The current O_3 concentrations remain alarmingly high in China, particularly in its developed eastern regions. The TP plays a crucial role in influencing climate change and subsequently affecting the photochemical production of O_3 in downstream EC. However, the link between TP and changes in O_3 concentrations has not been extensively studied. Utilizing the CHAP MDA8 O_3 dataset and ERA5 meteorological reanalysis data for 1980–2020, the interannual variations in warm season O_3 pollution over EC associated with springtime TP thermal forcing were investigated. This climatic study on O_3 pollution in EC connecting the TP thermal forcing could have the implication in improving long-term prediction of O_3 pollution application and forming the O_3 control strategy with the spatial disparities of TP effects on regional change of atmospheric environment in China.

The spatiotemporal characteristics of O_3 pollution during the warm seasons of 1980–2020 show significant spatial heterogeneity over the EC region. The six densely populated subregions exhibited relatively serious O_3 pollution, with the NCP experiencing the highest average MDA8 O_3 concentrations. Over the past 41 years, most areas in EC have experienced a progressive increase in O_3 pollution, with the PRD demonstrating the most pronounced increasing trend. Consequently, for the NCP and PRD, located in northern and southern EC, respectively, the O_3 pollution change with the TP thermal effect warrants attention.

The composite and correlation analyses indicated that strong springtime TP thermal forcing led to more and less O_3 pollution in the northern and southern EC regions, respectively. The subsequent EOF analysis further confirmed the close connection between the TP thermal effect and the EOF2 mode with a dipole spatial pattern. Moreover, different areas in EC have varying key sources of Q1 over the TP, depending on their locations and orientations to the large topography of the TP. Considering the spatially heterogeneous nature of interannual changes in the springtime thermal forcing over the TP, the key atmospheric heat sources identified in this study could be used in the more effective and fine prediction of O_3 pollution in major air pollution regions.

The different impacts of TP thermal forcing on meteorological anomalies determined the dipole spatial pattern of the MDA8 O_3 anomalies. In northern EC, strong TP thermal forcing triggered a significant anomalous high-pressure center accompanied by an anticyclone, resulting in an enhanced downdraft, reduced TCC, and increased SSR and T2, which were conducive to the anomalous increase in surface O_3 concentrations. Conversely, in southern EC, the influence of contrasting meteorological conditions driven by the strong thermal forcing of the TP reduced MDA8 O_3 concentrations.

However, climatic systems are complex and variable. Other climatic factors can also influence O_3 concentrations, such as the El Niño-Southern Oscillation (Yang et al., 2022), quasi-biennial oscillation (Li et al., 2023), and the sea surface temperature anomalies in the western Indian Ocean, western Pacific Ocean, and Ross Sea (Gao et al., 2023). In future studies, the combined effects of multiple climatic factors should be considered to obtain a more comprehensive understanding. Furthermore, our current analysis indicated the more significant impacts of the 1–4 year interannual variations in springtime TP heat source on the regional O_3 pollution. The effect of interdecadal variations and other scales of variations in TP heat source on regional O_3 pollution over China could be investigated in further studies. The local photochemical O_3 production plays an important role in interannual variations of regional O_3 pollution, especially in the precursor emission source regions NEC, NCP, SB, CC, YRD, and PRD. In addition, regional transport and dry/wet deposition could also affect the O_3 changes, which we would further examine and quantify the impacts with comprehensive observational data and modeling processes of atmospheric physics and chemistry.

Owing to the scarce observation network and complicated terrain and topography, there are deviations in the reanalysis data for the TP. Moreover, long-term and large-scale O_3 observational data are also lacking in China. Consequently, the climate modulation of air pollution requires further investigation with more accurate observational data of meteorology and the environment and climate models with more comprehensive processes of atmospheric physics and chemistry.

CRediT authorship contribution statement

Qingjian Yang: Writing – original draft, Methodology, Investigation, Data curation. **Tianliang Zhao:** Writing – review & editing, Methodology, Conceptualization. **Yongqing Bai:** Writing – review & editing, Methodology, Conceptualization. **Jing Wei:** Data curation. **Xiaoyun Sun:** Writing – review & editing. **Zhijie Tian:** Investigation, Conceptualization. **Jun Hu:** Investigation, Conceptualization. **Xiaodan Ma:** Investigation, Conceptualization. **Yuehan Luo:** Investigation, Conceptualization. **Weikang Fu:** Investigation, Conceptualization. **Kai Yang:** Investigation, Conceptualization.

Declaration of competing interest

The authors declare no competing financial interests or personal relationships that could have influenced the work reported in this article.

Data availability

Data will be made available on request.

Acknowledgment

This research was supported by the National Natural Science Foundation of China (42275196), the National Key Research and Development Program of China (2022YFC3701204), and the Postgraduate Research and Practice Innovation Program of Jiangsu Province (KYCX23_1317).

Appendix A. Supplementary data

Supplementary data to this article can be found online at https://doi.org/10.1016/j.scitotenv.2024.171527.

References

Anctil, F., Coulibaly, P., 2004. Wavelet analysis of the interannual variability in southern Québec streamflow. J. Climate 17, 163–173. https://doi.org/10.1175/1520-0442(2004)017<0163:WAOTIV>2.0.CO;2.

Arshinova, V., Belan, B., Lapchenko, V., Lapchenko, E., Rasskazchikova, T., Savkin, D., Sklyadneva, T., Tolmachev, G., Fofonov, A., 2019. Changes in surface ozone concentration during precipitation. Atmospheric and Oceanic Optics 32, 671–679.

Bao, Q., Wang, B., Liu, Y., Wu, G., 2008. The impact of the Tibetan Plateau warming on the East Asian summer monsoon—A study of numerical simulation. Chin. J. Atmos. Sci. 32 (5), 997–1005.

Butterworth, S., 1930. On the theory of filter amplifiers. Wireless Engineer 7, 536–541.

Coulibaly, P., Anctil, F., Rasmussen, P., Bobée, B., 2000. A recurrent neural networks approach using indices of low-frequency climatic variability to forecast regional annual runoff. Hydrol. Process. 14, 2755–2777. https://doi.org/10.1002/1099-1085(20001030)14:15<2755::AID-HYP90>3.0.CO;2-9.

Cui, Y., Duan, A., Liu, Y., Wu, G., 2015. Interannual variability of the spring atmospheric heat source over the Tibetan plateau forced by the North Atlantic SSTA. Climate Dynam. 45, 1617–1634. https://doi.org/10.1007/s00382-014-2417-9.

Duan, A., Zhang, P., 2022. Interannual variability of atmospheric heat source over the Tibetan plateau and its driving factors. Chin. J. Atmos. Sci. 46, 455–472.

Duan, A., Li, F., Wang, M., Wu, G., 2011. Persistent weakening trend in the spring sensible heat source over the Tibetan plateau and its impact on the Asian summer monsoon. J. Climate 24, 5671–5682. https://doi.org/10.1175/JCLI-D-11-00052.1.

Duan, A.M., Wu, G.X., 2005. Role of the Tibetan plateau thermal forcing in the summer climate patterns over subtropical Asia. Climate Dynam. 24, 793–807. https://doi.org/10.1007/s00382-004-0488-8.

Feng, Z., Hu, E., Wang, X., Jiang, L., Liu, X., 2015. Ground-level O3 pollution and its impacts on food crops in China: a review. Environ. Pollut. 199, 42–48.

Gao, M., Wang, F., Ding, Y., Wu, Z., Xu, Y., Lu, X., Wang, Z., Carmichael, G.R., McElroy, M.B., 2023. Large-scale climate patterns offer preseasonal hints on the co-occurrence of heat wave and O3 pollution in China. Proc. Natl. Acad. Sci. 120, e2218274120 https://doi.org/10.1073/pnas.2218274120.

Ge, J., You, Q., Zhang, Y., 2019. Effect of Tibetan plateau heating on summer extreme precipitation in eastern China. Atmos. Res. 218, 364–371. https://doi.org/10.1016/j.atmosres.2018.12.018.

Gouirand, I., Jury, M.R., Sing, B., 2012. An analysis of low- and high-frequency summer climate variability around the Caribbean Antilles. J. Climate 25, 3942–3952. https://doi.org/10.1175/JCLI-D-11-00269.1.

Gu, Y., Li, K., Xu, J., Liao, H., Zhou, G., 2020. Observed dependence of surface ozone on increasing temperature in Shanghai, China. Atmos. Environ. 221, 117108.

Haman, C., Couzo, E., Flynn, J., Vizuete, W., Heffron, B., Lefer, B., 2014. Relationship between boundary layer heights and growth rates with ground-level ozone in Houston. Texas. Journal of Geophysical Research: Atmospheres 119. https://doi.org/10.1002/2013JD020473.

Han, H., Liu, J., Shu, L., Wang, T., Yuan, H., 2020. Local and synoptic meteorological influences on daily variability in summertime surface ozone in eastern China. Atmospheric Chemistry and Physics 20, 203–222. https://doi.org/10.5194/acp-20-203-2020.

Han, Y., Jiang, D., Si, D., Ma, Y., Ma, W., 2024. Time-lagged effects of the spring atmospheric heat source over the Tibetan plateau on summer precipitation in Northeast China during 1961–2020: role of soil moisture. Adv. Atmos. Sci. 1–12.

Hannachi, A., Jolliffe, I.T., Stephenson, D.B., 2007. Empirical orthogonal functions and related techniques in atmospheric science: a review. Int. J. Climatol. 27, 1119–1152. https://doi.org/10.1002/joc.1499.

He, L., Wei, J., Wang, Y., Shang, Q., Liu, J., Yin, Y., Frankenberg, C., Jiang, J.H., Li, Z., Yung, Y.L., 2022. Marked impacts of pollution mitigation on crop yields in China. Earth's Future 10. https://doi.org/10.1029/2022EF002936.

He, X., Pang, S., Ma, J., Zhang, Y., 2017. Influence of relative humidity on heterogeneous reactions of O3 and O3/SO2 with soot particles: potential for environmental and health effects. Atmos. Environ. 165, 198–206.

Hersbach, H., Bell, B., Berrisford, P., Hirahara, S., Horányi, A., Muñoz-Sabater, J., Nicolas, J., Peubey, C., Radu, R., Schepers, D., Simmons, A., Soci, C., Abdalla, S., Abellan, X., Balsamo, G., Bechtold, P., Biavati, G., Bidlot, J., Bonavita, M., De Chiara, G., Dahlgren, P., Dee, D., Diamantakis, M., Dragani, R., Flemming, J., Forbes, R., Fuentes, M., Geer, A., Haimberger, L., Healy, S., Hogan, R.J., Hólm, E., Janisková, M., Keeley, S., Laloyaux, P., Lopez, P., Lupu, C., Radnoti, G., de Rosnay, P., Rozum, I., Vamborg, F., Villaume, S., Thépaut, J.-N., 2020. The ERA5 global reanalysis. Q. J. Roy. Meteorol. Soc. 146, 1999–2049. https://doi.org/10.1002/qj.3803.

Jacob, D.J., Winner, D.A., 2009. Effect of climate change on air quality. Atmos. Environ. 43, 51–63.

Kou, W., Gao, Y., Zhang, S., Cai, W., Geng, G., Davis, S.J., Wang, Hong, Guo, X., Cheng, W., Zeng, X., Ma, M., Wang, Houwen, Wang, Q., Yao, X., Gao, H., Wu, L., 2023. High downward surface solar radiation conducive to ozone pollution more frequent under global warming. Sci. Bull. 68 (4), 388–392.

Lee, Y.C., Shindell, D.T., Faluvegi, G., Wenig, M., Lam, Y.F., Ning, Z., Hao, S., Lai, C.S., 2014. Increase of ozone concentrations, its temperature sensitivity and the precursor factor in South China. Tellus B: Chemical and Physical Meteorology 66, 23455. https://doi.org/10.3402/tellusb.v66.23455.

Li, K., Jacob, D.J., Liao, H., Zhu, J., Shah, V., Shen, L., Bates, K.H., Zhang, Q., Zhai, S., 2019a. A two-pollutant strategy for improving ozone and particulate air quality in China. Nat. Geosci. 12, 906–910.

Li, K., Jacob, D.J., Liao, H., Shen, L., Zhang, Q., Bates, K.H., 2019b. Anthropogenic drivers of 2013–2017 trends in summer surface ozone in China. Proc. Natl. Acad. Sci. 116, 422–427. https://doi.org/10.1073/pnas.1812168116.

Li, K., Jacob, D.J., Shen, L., Lu, X., De Smedt, I., Liao, H., 2020. Increases in surface ozone pollution in China from 2013 to 2019: anthropogenic and meteorological influences. Atmospheric Chemistry and Physics 20, 11423–11433. https://doi.org/10.5194/acp-20-11423-2020.

Li, M., Yu, S., Chen, X., Li, Z., Zhang, Y., Wang, L., Liu, W., Li, P., Lichtfouse, E., Rosenfeld, D., 2021. Large scale control of surface ozone by relative humidity observed during warm seasons in China. Environ. Chem. Lett. 19, 3981–3989.

Li, M., Yang, Y., Wang, H., Li, H., Wang, P., Liao, H., 2023. Summertime ozone pollution in China affected by stratospheric quasi-biennial oscillation. Atmospheric Chemistry and Physics 23, 1533–1544. https://doi.org/10.5194/acp-23-1533-2023.

Lin, J.-T., Patten, K.O., Hayhoe, K., Liang, X.-Z., Wuebbles, D.J., 2008. Effects of future climate and biogenic emissions changes on surface ozone over the United States and China. J. Appl. Meteorol. Climatol. 47, 1888–1909. https://doi.org/10.1175/2007JAMC1681.1.

Liu, X., Li, W., Xu, H., Wu, G., 2007. The effect of Tibetan plateau heating on the east Asian summer precipitation. Plateau Meteorology 26, 1287–1292.

Lu, X., Zhang, L., Shen, L., 2019. Meteorology and climate influences on tropospheric ozone: a review of natural sources, chemistry, and transport patterns. Curr. Pollut. Rep. 5, 238–260.

Ma, D., Wang, T., Wu, H., Qu, Y., Liu, Jian, Liu, Jane, Li, S., Zhuang, B., Li, M., Xie, M., 2023. The effect of anthropogenic emission, meteorological factors, and carbon dioxide on the surface ozone increase in China from 2008 to 2018 during the East Asia summer monsoon season. Atmospheric Chemistry and Physics 23, 6525–6544. https://doi.org/10.5194/acp-23-6525-2023.

Ma, M., Gao, Y., Wang, Y., Zhang, S., Leung, L.R., Liu, C., Wang, S., Zhao, B., Chang, X., Su, H., 2019. Substantial ozone enhancement over the North China plain from increased biogenic emissions due to heat waves and land cover in summer 2017. Atmospheric Chemistry and Physics 19, 12195–12207.

Ma, X., Yin, Z., 2021. Dipole pattern of summer ozone pollution in the east of China and its connection with climate variability. Atmospheric Chemistry and Physics 21, 16349–16361.

Ma, Y., Ma, W., Zhong, L., Hu, Z., Li, M., Zhu, Z., Han, C., Wang, B., Liu, X., 2017. Monitoring and modeling the Tibetan Plateau's climate system and its impact on East Asia. Sci. Rep. 7, 1–6.

Nuvolone, D., Petri, D., Voller, F., 2018. The effects of ozone on human health. Environ. Sci. Pollut. Res. 25, 8074–8088.

Ping, Z., Longxun, C., 2001. Interannual variability of atmospheric heat source/sink over the Qinghai—Xizang (Tibetan) plateau and its relation to circulation. Adv. Atmos. Sci. 18, 106–116. https://doi.org/10.1007/s00376-001-0007-3.

Shen, L., Mickley, L.J., Gilleland, E., 2016. Impact of increasing heat waves on U.S. ozone episodes in the 2050s: results from a multimodel analysis using extreme value theory. Geophys. Res. Lett. 43, 4017–4025. https://doi.org/10.1002/2016GL068432.

Sifuzzaman, M., Islam, R., Ali, M., 2009. Application of Wavelet Transform and its Advantages Compared to Fourier Transform. J. Phys, Sci, p. 13.

Sillman, S., 2003. Tropospheric ozone and photochemical smog. Environmental geochemistry 9, 407–431.

Sun, S., Guan, Z., 2021. Rossby wave packets in the upper troposphere and their associations with climatological summertime daily precipitation in MLRYR of China. Atmos. Sci. Lett. 22, e1023 https://doi.org/10.1002/asl.1023.

Sun, X., Zhao, T., Xu, X., Bai, Y., Zhao, Y., Ma, X., Shu, Z., Hu, W., 2023. Identifying the impacts of warming anomalies in the Arctic region and the Tibetan plateau on PM2.5 pollution and regional transport over China. Atmos. Res. 294, 106966 https://doi.org/10.1016/j.atmosres.2023.106966.

Tang, C., Zhu, F., Wei, Y., Tian, X., Yang, J., Zhao, F., 2023. Study of time-frequency domain characteristics of the Total column ozone in China based on wavelet analysis. Atmosphere 14, 941. https://doi.org/10.3390/atmos14060941.

Torrence, C., Compo, G.P., 1998. A practical guide to wavelet analysis. Bull. Am. Meteorol. Soc. 79, 61–78. https://doi.org/10.1175/1520-0477(1998)079<0061:APGTWA>2.0.CO;2.

Wang, M., Huang, T., Wong, D.C., Ho, K.F., Dong, G., Yim, S.H., 2021a. A new approach for health-oriented ozone control strategy: Adjoint-based optimization of NOx emission reductions using metaheuristic algorithms. J. Clean. Prod. 312, 127533 https://doi.org/10.1016/j.jclepro.2021.127533.

Wang, T., Xue, L., Feng, Z., Dai, J., Zhang, Y., Tan, Y., 2022. Ground-level ozone pollution in China: a synthesis of recent findings on influencing factors and impacts. Environ. Res. Lett. 17, 063003 https://doi.org/10.1088/1748-9326/ac69fe.

Wang, Y., Gao, W., Wang, S., Song, T., Gong, Z., Ji, D., Wang, L., Liu, Z., Tang, G., Huo, Y., 2020. Contrasting trends of PM2. 5 and surface-ozone concentrations in China from 2013 to 2017. Natl. Sci. Rev. 7, 1331–1339. https://doi.org/10.1093/nsr/nwaa032.

Wang, Y., Yan, Y., Duan, K., Kong, S., Lin, J., Zheng, H., Song, A., Zhang, Z., 2021b. Effect of springtime thermal forcing over Tibetan plateau on summertime ozone in Central China during the period 1950–2019. Atmos. Res. 261, 105735 https://doi.org/10.1016/j.atmosres.2021.105735.

Wang, Z., Duan, A., Wu, G., 2014. Time-lagged impact of spring sensible heat over the Tibetan plateau on the summer rainfall anomaly in East China: case studies using the WRF model. Climate Dynam. 42, 2885–2898. https://doi.org/10.1007/s00382-013-1800-2.

Wei, J., Li, Z., Li, K., Dickerson, R.R., Pinker, R.T., Wang, J., Liu, X., Sun, L., Xue, W., Cribb, M., 2022. Full-coverage mapping and spatiotemporal variations of ground-level ozone (O3) pollution from 2013 to 2020 across China. Remote Sens. Environ. 270, 112775 https://doi.org/10.1016/j.rse.2021.112775.

Wu, G., Liu, Y., Zhang, Q., Duan, A., Wang, T., Wan, R., Liu, X., Li, W., Wang, Z., Liang, X., 2007. The influence of mechanical and thermal forcing by the Tibetan plateau on Asian climate. J. Hydrometeorol. 8, 770–789.

Wu, G., Liu, Y., Dong, B., Liang, X., Duan, A., Bao, Q., Yu, J., 2012a. Revisiting Asian monsoon formation and change associated with Tibetan plateau forcing: I. Formation. Climate dynamics 39, 1169–1181.

Wu, G., Liu, Y., He, B., Bao, Q., Duan, A., Jin, F.-F., 2012b. Thermal controls on the Asian summer monsoon. Sci. Rep. 2, 1–7.

Wu, G., Liu, Y., He, B., Bao, Q., Wang, Z., 2018. Review of the impact of the Tibetan plateau sensible heat driven air-pump on the Asian summer monsoon. Chin. J. Atmos. Sci. 42, 488–504.

Xu, X., Lu, C., Ding, Y., Shi, X., Guo, Y., Zhu, W., 2013. What is the relationship between China summer precipitation and the change of apparent heat source over the Tibetan plateau? Atmos. Sci. Lett. 14, 227–234. https://doi.org/10.1002/asl2.444.

Xu, X., Zhao, T., Liu, F., Gong, S.L., Kristovich, D., Lu, C., Guo, Y., Cheng, X., Wang, Y., Ding, G., 2016. Climate modulation of the Tibetan plateau on haze in China. Atmos. Chem. Phys. 16, 1365–1375. https://doi.org/10.5194/acp-16-1365-2016.

Yanai, M., Esbensen, S., Chu, J.-H., 1973. Determination of bulk properties of tropical cloud clusters from large-scale heat and moisture budgets. J. Atmos. Sci. 30, 611–627.

Yanai, M., Li, C., Song, Z., 1992. Seasonal heating of the Tibetan plateau and its effects on the evolution of the Asian summer monsoon. Journal of the meteorological Society of Japan. Ser. II 70, 319–351.

Yang, X., Zeng, G., Zhang, G., Li, J., Li, Z., Hao, Z., 2021. Interdecadal variations of different types of summer heat waves in Northeast China associated with AMO and PDO. J. Climate 34, 7783–7797. https://doi.org/10.1175/JCLI-D-20-0939.1.

Yang, Y., Li, M., Wang, H., Li, H., Wang, P., Li, K., Gao, M., Liao, H., 2022. ENSO modulation of summertime tropospheric ozone over China. Environ. Res. Lett. 17, 034020 https://doi.org/10.1088/1748-9326/ac54cd.
You, J., Liang, X., 2017. Reconstructing the MJO with multiscale window transform. Trans. Atmos. Sci. 40, 25–35.
Yue, X., Unger, N., Harper, K., Xia, X., Liao, H., Zhu, T., Xiao, J., Feng, Z., Li, J., 2017. Ozone and haze pollution weakens net primary productivity in China. Atmospheric Chemistry and Physics 17, 6073–6089.
Zhang, J., Liu, C., Chen, H., 2018. The modulation of Tibetan plateau heating on the multi-scale northernmost margin activity of East Asia summer monsoon in northern China. Global Planet. Change 161, 149–161.
Zhao, P., Zhou, Z., Liu, J., 2007. Variability of Tibetan spring snow and its associations with the hemispheric extratropical circulation and east Asian summer monsoon rainfall: an observational investigation. J. Climate 20, 3942–3955. https://doi.org/10.1175/JCLI4205.1.
Zhao, Y., Duan, A., Wu, G., 2018. Interannual variability of late-spring circulation and Diabatic heating over the Tibetan plateau associated with Indian Ocean forcing. Adv. Atmos. Sci. 35, 927–941. https://doi.org/10.1007/s00376-018-7217-4.
Zhu, A., Xu, H., Deng, J., Ma, J., Li, S., 2021. El Niño–Southern Oscillation (ENSO) effect on interannual variability in spring aerosols over East Asia. Atmospheric Chemistry and Physics 21, 5919–5933. doi:https://doi.org/10.5194/acp-21-5919-2021.